Black hole-neutron star mergers in Einstein-scalar-Gauss-Bonnet gravity

Maxence Corman[1,*] and William E. East[2,†]

[1]*Max Planck Institute for Gravitational Physics (Albert Einstein Institute), D-14476 Potsdam, Germany*
[2]*Perimeter Institute for Theoretical Physics, Waterloo, Ontario N2L 2Y5, Canada*

(Received 18 June 2024; accepted 27 September 2024; published 24 October 2024)

Gravitational wave observations of black hole-neutron star binaries, particularly those where the black hole has a lower mass compared to other observed systems, have the potential to place strong constraints on modifications to general relativity that arise at small curvature length scales. Here we study the dynamics of black hole-neutron star mergers in shift-symmetric Einstein-scalar-Gauss-Bonnet gravity, a representative example of such a theory, by numerically evolving the full equations of motion. We consider quasi-circular binaries with different mass-ratios that are consistent with recent gravitational wave observations, including cases with and without tidal disruption of the star, and quantify the impact of varying the coupling controlling deviations from general relativity on the gravitational wave signal and scalar radiation. We find that the main effect on the late inspiral is the accelerated frequency evolution compared to general relativity, and that—even considering Gauss-Bonnet coupling values approaching those where the theory breaks down—the impact on the merger gravitational wave signal is mild, predominately manifesting as a small change in the amplitude of the ringdown. We compare our results to current post-Newtonian calculations and find consistency throughout the inspiral.

DOI: 10.1103/PhysRevD.110.084065

I. INTRODUCTION

The growing number of gravitational wave observations [1–4] has opened up new opportunities to probe the strong gravity regime governing the coalescence of compact binary systems, marking a new chapter for tests of general relativity (GR) [5–15]. To robustly test GR in this highly dynamical and nonlinear regime, we need accurate predictions in modified theories of gravity that cover the full inspiral, merger, and ringdown of compact object binaries.

Many proposed modifications to GR rely on effective field theory arguments [16,17], and hence result from adding additional curvature terms to the Einstein-Hilbert action multiplied by some coupling constants with (positive) dimensions of length. Examples include not only the most generic Horndeski theories [18] and dynamical Chern-Simons gravity [19], but also theories that add higher-dimensional curvature operators without introducing new light degrees of freedom [20,21]. It is then natural to expect that such alternative theories of gravity exhibit the strongest deviations in the presence of the shortest curvature length scales. This makes the smallest mass compact objects ideal probes for finding evidence of, or constraining such theories.

In this paper, we study how black hole-neutron star (BHNS) mergers can be used to probe a representative modified theory of gravity introducing modifications to GR at small curvature length scales, namely Einstein-scalar-Gauss-Bonnet (EsGB) gravity. An interesting aspect of EsGB gravity is that neutron stars carry no scalar charge, while black holes do [22–27]. This means that unlike Damour-Esposito-Farese scalar-tensor (ST) theories [28], where neutron stars develop a scalar charge and black holes do not [29–32], EsGB gravity evades binary pulsar system constraints based on dipolar radiation [5,33],[1] and instead one has to search for observational signatures in other ways, such as through compact object merger dynamics. An important feature of EsGB gravity is the emission of scalar radiation in addition to the usual tensor radiation found in GR [37]. Similar to ST theories, the leading scalar radiation is dipolar, and thus dominates over quadrupolar gravitational waves at low frequencies [38]. The strength of

*Contact author: maxence.corman@aei.mpg.de
†Contact author: weast@perimeterinstitute.ca

[1]We note that while ST theories are strongly constrained by binary pulsar observations [5,33], there are examples where the neutron star undergoes *spontaneous scalarization* (dynamical [34,35] or induced [28,29]) or the scalar field is massive [36], which suppresses effects at the separations currently observed, hence avoiding current constraints.

this radiation depends not only on the scalar charge of the compact objects, which is inversely proportional to the square of the smallest mass black hole in the system, but also on the square of the difference between the charges of the constituent objects [38]. Therefore, if two objects possess similar charges, such as in an equal or near equal mass binary black hole merger, the dipolar radiation will be suppressed. Conversely, the strongest constraints on EsGB gravity, as well as ST theories, can come from a mixed binary consisting of ideally a small black hole and a neutron star, as only one of them carries a scalar charge. Recently, in Ref. [39], fully nonlinear numerical simulations were used to study a BHNS merger in ST theory,[2] focusing on how the gravitational wave emission is affected by the spontaneous scalarization of the neutron star. Considering a binary with parameters consistent with the gravitational wave event GW200115 [40], Ref. [39] found that the ST system inspiraled faster than its GR counterpart due to the emission of scalar radiation, showing good agreement with predictions from post-Newtonian (PN) theory during the inspiral.

In the third observing run of the Advanced LIGO [41], Advanced Virgo [42], and KAGRA [43,44] network of gravitational wave detectors, the LIGO-Virgo detectors observed GW200105 and GW200115, the first gravitational wave detections from the mergers of BHNS systems [40]. By adopting the leading order (dipolar) PN correction, Ref. [45] derived the strongest bound on coupling constant of theory at that time to be on the order of kilometer or less. This was achieved through a Bayesian Markov-chain Monte Carlo analysis combining GW200105, GW200115, GW190814 [46],[3] and selected binary black hole events. More recently, the LIGO-Virgo-KAGRA Collaboration (LVK) reported the observation of a compact object binary merger in May 2023, GW230529, with component masses $3.6^{+0.8}_{-1.2}M_\odot$ and $1.4^{+0.6}_{-0.2}M_\odot$, the most probable interpretation of which is the coalescence of a black hole in the lower mass gap and a neutron star [47]. To verify whether GW230529 is consistent with GR, the LVK collaboration performed so-called parametrized tests, searching for parametric deviations to the gravitational wave phase during the inspiral, specifically using the TIGER [48,49] and FTI [50] frameworks. For all waveform models and PN orders so far considered, GW230529 was found to be consistent with GR, with constraints on the -1PN (dipolar) coefficient being an order of magnitude tighter than previous bounds for BHNS and binary black hole (BBH) mergers reported by the collaboration [47]. Applying the same methods as Ref. [45] to GW230529, Ref. [51] improved the bounds on coupling constant by a factor of approximately four. Alternatively, mapping the -1PN constraints from FTI tests to a constraint on the coupling constant in EsGB gravity, Ref. [52] also obtained a tighter bound on coupling constant. With upcoming improvements in the sensitivity of the LVK gravitational wave detectors [53], as well as future third-generation ground-based detectors [54,55], it is thus timely and vital to provide predictions of gravitational wave signals from BHNS binaries in EsGB gravity. Although significant progress has been made in modeling compact object mergers in EsGB gravity using PN theory [37,38,56–58], as one approaches the merger, PN theory breaks down, and numerical relativity is required. For EsGB gravity, numerical relativity has been used to study binary neutron star and binary black hole systems, solving the full equations [59–64], and using a decoupling or order-by-order approximation [65–68]. See also Ref. [69] for a comparison of the different approaches for treating modifications to full general relativity that have been used to study binary black hole mergers.

However, a simulation of a BHNS merger in EsGB gravity is still missing. In this work, we aim to fill this gap and take advantage of recent advances in solving the full equations of shift-symmetric EsGB gravity to study the nonlinear dynamics of BHNS mergers in this theory. In particular, we make use of the modified harmonic formulation [70,71] and methods developed in Refs. [59,60,62] for evolving black holes and neutron stars in shift-symmetric EsGB gravity. We focus on how the gravitational wave emission is impacted by the presence of an additional energy dissipation channel.

Motivated by the LVK observations, we consider two binary systems, namely one consistent with GW200115, and another with GW230529. For the latter, we choose an equation of state (EOS) and mass ratio so that the neutron star is tidally disrupted. For coupling values comparable to the upper bound obtained from GW200115, we find a noticeable dephasing in the gravitational wave signal compared to GR in the inspiral. However, in the last few orbits, the rate of dephasing becomes small (even being consistent with zero or indicating a slower inspiral rate for EsGB compared to GR to within the numerical errors). In part due to this suppression, we find the PN approximation to be consistent with our results into the late inspiral. We also study the effect of modifications to GR on the merger and ringdown signal. We find that the effect on the peak amplitude of the gravitational wave signal is small, with the relative change in the ringdown frequency being at most on the order of $\sim 1\%$ for the largest couplings we consider, while the amplitude of ringdown signal can vary by $\sim 10\%$ for the GW200115-like binary. We observe a amplification (or suppression) in the amplitude of ringdown gravitational wave signal with increasing coupling when neutron star is (or not) tidally disrupted. We conjecture that the amplification is due to the neutron star being more compact and less strongly tidally disrupted for larger couplings.

[2]ST theories do not modify the principal part of the Einstein equations and can be evolved in the same way.

[3]This event is consistent with both a binary black hole and a BHNS binary.

Finally, in the case where neutron star is tidally disrupted, we find that the amount of mass remaining outside black hole after the merger decreases slightly with increasing coupling when fixing the EOS.

The remainder of this paper is organized as follows. We review the theory we consider, shift-symmetric EsGB gravity, in Sec. II. We describe our numerical methods for evolving this theory coupled to hydrodynamics and analyzing the results in Sec. III. Results from our study of BHNS binaries in shift-symmetric EsGB gravity are presented in Sec. IV. We discuss these results and conclude in Sec. V. We discuss the accuracy our simulations in the Appendix. We use geometric units: $G = c = 1$, a metric sign convention of $-+++$, and lower case Latin letters to index spacetime indices. The Riemann tensor is $R^a{}_{bcd} = \partial_c \Gamma^a_{db} - \cdots$.

II. SHIFT-SYMMETRIC EINSTEIN SCALAR GAUSS BONNET GRAVITY

The action for shift-symmetric EsGB gravity is

$$S = \frac{1}{16\pi}\int d^4x\sqrt{-g}(R - (\nabla\phi)^2 + 2\lambda\phi\mathcal{G}) + S_{\rm matter}, \quad (1)$$

where g is the determinant of spacetime metric and $\mathcal{G}$ is the Gauss-Bonnet scalar

$$\mathcal{G} \equiv R^2 - 4R_{ab}R^{ab} + R_{abcd}R^{abcd}. \quad (2)$$

Here, λ is a constant coupling parameter that, in geometric units, has dimensions of length squared, ϕ is the scalar field and $S_{\rm matter}$ is the action for any other matter (in our case the neutron star fluid). As the Gauss-Bonnet scalar $\mathcal{G}$ is a total derivative in four dimensions, we see that the action is preserved up to total derivatives under constant shifts in the scalar field: $\phi \to \phi +$ constant.

The covariant equations of motion for shift-symmetric EsGB gravity are

$$\Box\phi + \lambda\mathcal{G} = 0, \quad (3)$$

$$R_{ab} - \frac{1}{2}g_{ab}R + 2\lambda\delta^{efcd}_{ijg(a}g_{b)d}R^{ij}{}_{ef}\nabla^g\nabla_c\phi = 8\pi T_{ab}, \quad (4)$$

where δ^{abcd}_{efgh} is the generalized Kronecker delta tensor and $T_{ab} = T^{\rm SF}_{ab} + T^{\rm matter}_{ab}$ with

$$T^{\rm SF}_{ab} \equiv \frac{1}{8\pi}\left(\nabla_a\phi\nabla_b\phi - \frac{1}{2}(\nabla\phi)^2 g_{ab}\right). \quad (5)$$

We do not introduce any nonminimal coupling for the matter in the Einstein frame, and the equations of motion for the matter terms are the same as in GR.

Schwarzschild and Kerr black holes are not stationary solutions in this theory: if one begins with such vacuum initial data, the black holes will dynamically develop stable scalar clouds (hair). The end state is a black hole with nonzero scalar charge $Q_{\rm SF}$, such that at large radius the scalar field falls of like $\phi = Q_{\rm SF}/r + \mathcal{O}(1/r^2)$. Furthermore, studies have found that stationary solutions exist, as long as the coupling normalized by the total black hole mass as measured at infinity m, λ/m^2, is sufficiently small [24,25,60,72]. In particular, regularity of black hole solutions and hyperbolicity of the theory set $\lambda/m^2 \lesssim 0.23$ for nonspinning black holes, [25,72].

Neutron stars, in contrast to black holes, do not have a scalar charge in EsGB gravity [37,56]. However, it is important to note that despite not having a scalar charge, a neutron star in EsGB gravity will still be surrounded by a scalar cloud (sourced by the Gauss-Bonnet invariant). The lack of scalar charge arises because the scalar field decays much more rapidly than with $1/r$, as would be required for the neutron star to have a scalar charge. Neutron stars in shift-symmetric EsGB gravity were studied (restricting to spherical symmetry) in Ref. [73], where it was numerically found that (independently of the equation of state of neutron star) turning on the EsGB coupling tends to reduce the maximum gravitational mass or increase the central density when a solution exists. It was further analytically shown that depending on the value of the coupling and neutron star EOS, there is a maximum central density beyond which no spherically symmetric perfect fluid solutions can be constructed.

In general, the equations of motion for EsGB gravity can only be evolved in time in a well-posed manner for weakly-coupled solutions [60,61,70,71,74].[4] In earlier studies of collapse and black hole and neutron star binaries in EsGB gravity, it was found that when the coupling of the theory is made too large, the compact objects can evolve from an initial weakly coupled state, to a strongly coupled state, where the hyperbolicity of the evolution equations breaks down, although approaching this limit does not appear to be preceded by any singular behavior developing in the metric or scalar field [59,60,62,74–77]. Here we find evidence that this breakdown happens in BHNS mergers not only when a black hole scalarizes, but also sometimes when the scalar field in the neutron star grows in magnitude, leading to an increase in the star's density. However, this breakdown occurs for coupling values comparable to or larger than the best existing constraints on EsGB gravity and approaching this limit does not appear to be preceded by dramatically different spacetime and/or scalar field dynamics.

III. METHODS

A. Evolution equations and code overview

We numerically evolve the full shift-symmetric EsGB equations of motion using the modified generalized

[4]Weak coupling means that the Gauss-Bonnet corrections to the equations of motion remain sufficiently small compared to the leading two-derivative terms. This is consistent with strong-field black hole dynamics provided the size of the smallest black hole in the system is larger than the length scale.

harmonic formulation [70,71]. We use similar choices for the gauge and numerical parameters as in Ref. [60]. We model the neutron star using ideal hydrodynamics. The Euler equations are the same as in GR, and evolved using the hydrodynamics code described in Ref. [78]. We use the same methods and parameters for evolving BHNS binaries as in Ref. [79]. Our simulations use box-in-box adaptive mesh refinement provided by the PAMR library [80]. We typically use seven levels of mesh refinement in our simulations, unless otherwise noted. We provide details on numerical resolution and convergence in the Appendix.

B. Initial data and cases considered

We use quasicircular BHNS binary initial data constructed with the Frankfurt University/Kadath (FUKA) Initial Data code suite [81], which is based on an extended version of the KADATH spectral solver library [82]. We choose $\phi = \partial_t \phi = 0$ on the initial time slice, in which case the constraint equations of shift-symmetric EsGB gravity reduce to those of vacuum GR. We slowly ramp on the coupling of the theory as described in Appendix B of Ref. [83], in such a way that the scalar field grows on a timescale that is short compared with the orbital binary timescale. The set of hydrodynamical evolution equations are closed by an equation of state connecting pressure p to specific internal energy ϵ and rest mass density ρ, i.e., $p = p(\rho, \epsilon)$. Though in general it would be interesting to consider different EOSs in order to determine how this impacts the results and to test for possible degeneracies, for this first study we consider a single one for the neutron star. We use a cold piecewise polytropic EOS [84] approximating the ALF2 EOS [85] for the neutron star. This prototypical stiff EOS predicts the radius of a $1.4M_\odot$ neutron star to be $R_{1.4} \sim 12.32$ km [86], has a maximum mass of $\sim 2.0M_\odot$ for nonspinning stars [85], and is consistent with pulsar observations [87–91], with both electromagnetic and gravitational wave observations [92–97] of the binary neutron star event GW170817 [98], as well as the gravitational wave observations of GW190814 [99] and GW190425 [100]. Thermal effects are added to the zero-temperature polytrope with an additional pressure contribution of the form $p_{\rm th} = (\Gamma_{\rm th} - 1)\rho\epsilon$, where $\epsilon_{\rm th}$ denotes the excess specific energy compared to the cold value at the same density. We use $\Gamma_{\rm th} = 1.75$, motivated by studies comparing nonzero temperature EOSs such as Refs. [101,102].

The binary parameters we consider for one of the BHNS system we study are chosen to be consistent with GW200115 [40]. The source of GW200115 has component masses $5.7^{+1.8}_{-2.1}$ and $1.5^{0.7}_{-0.3} M_\odot$ at a 90% confidence level and mass ratio $q = 0.26^{0.35}_{-0.10}$. The primary spin has a negative spin projection onto the orbital angular momentum (anti-aligned spin), but is also consistent with zero spin $\chi_1 = 0.33^{+0.48}_{-0.29}$. The spin and tidal deformability of the neutron star were unconstrained, and no electromagnetic counterpart has been identified to date. We consider a nonrotating neutron star with gravitational mass $m_{\rm NS} = 1.5M_\odot$ and a nonspinning black hole with mass $m_{\rm BH} = 5.7M_\odot$. We consider two initial separations: $D = 10.35M$ and $D = 8.61M$, where $M = 7.2M_\odot$ is total mass of system. The systems undergo approximately 7 and 4.5 orbital periods, respectively, before merging in GR. For the longer inspiral, we consider two values of the coupling parameter, namely $\lambda/m_{\rm BH}^2 = (0, 0.1)$. For values much above the maximum value of the coupling we consider, we find that with these binary parameters the neutron star becomes ill-behaved, suggesting we are approaching the value where no spherically symmetric neutron star exists for this EOS. We estimate the initial orbital eccentricity to be $\sim 6 \times 10^{-3}$. For the shorter inspiral, we consider an additional coupling of $\lambda/m_{\rm BH}^2 = 0.05$.

The second system we consider has binary parameters consistent with the recent GW230529 event [47]. The source of GW230529 has component masses $3.6^{+0.8}_{-1.2} M_\odot$ and $1.4^{+0.6}_{-0.2} M_\odot$ and mass ratio $q = 0.39^{0.41}_{-0.12}$ at the 90% confidence level. The primary spin most likely has a negative component when projected onto the orbital angular momentum, but is also consistent with zero spin: $\chi_1 = 0.44^{+0.40}_{-0.37}$. The spin and tidal deformability of the neutron star were unconstrained, and no electromagnetic counterpart has been identified to date. Using the high-spin combined posterior samples, Ref. [47] found that the probability that the neutron star was tidally disrupted is 0.1, corresponding to an upper limit on the remnant baryon mass produced in the merger of $0.052M_\odot$ at the 99% confidence interval. Yet this source is the most probable of the BHNS events reported by the LVK to have undergone tidal disruption because of the increased symmetry in the component masses. We therefore consider a nonrotating neutron star with gravitational mass $m_{\rm NS} = 1.4M_\odot$ and a nonspinning black hole with a mass of $m_{\rm BH} = 3.5M_\odot$, so that for the EOS we choose the neutron star is tidally disrupted at merger. The initial separation is $D = 9.82M$, or approximately 5 orbits before merging in GR. We consider coupling values of $\lambda/m_{\rm BH}^2 = 0$, 0.1, and 0.15, where the maximum value of the coupling here approaches limit where hyperbolicity of black hole solution breaks down during scalarization process ($\lambda/m_{\rm BH}^2 \approx 0.23$).

For ease of comparisons with other works, we convert our coupling λ into $\alpha_{\rm GB} \equiv \lambda/\sqrt{8\pi}$ used in, e.g., Refs. [45,103].[5] Restoring physical units we have,

$$\sqrt{\alpha_{GB}} \approx 3.77 \text{ km} \left(\frac{\sqrt{\lambda}}{m_{\rm BH}}\right)\left(\frac{m_{\rm BH}}{5.7M_\odot}\right). \tag{6}$$

For reference, Ref. [45] sets a constraint of $\sqrt{\alpha_{\rm GB}} \lesssim 1.18$ km at a 90% confidence level by comparing

[5]However, several other studies (e.g., Refs. [65,104–106]) take conventions leading to a value of $\alpha_{\rm GB}$ that is $16\sqrt{\pi}\times$ times larger.

TABLE I. Summary of the parameters of the GW200115- and GW230529-like BHNS systems we consider. The black hole is nonspinning and has an irreducible mass $m_{\rm BH}$, while the neutron star has a gravitational mass $m_{\rm NS}$ with radius given by $R_{\rm NS}$. TD indicates whether neutron star is tidally disrupted or not before merger and $N^{\rm GR}_{\rm cycle}$ is the number of gravitational wave cycles before merger in GR. The coupling values we consider are denoted by $\sqrt{\alpha_{\rm GB}}$.

GW event	$m_{\rm BH}/M_\odot$	$m_{\rm NS}/M_\odot$	q	$R_{\rm NS}$/km	D/M	TD	$N^{\rm GR}_{\rm cycle}$	$\sqrt{\alpha_{\rm GB}}$/km
GW200115	5.7	1.5	0.26	12.3	10.35	No	7	$\{0, 1.19\}$
GW200115	5.7	1.5	0.26	12.3	8.61	No	4	$\{0, 0.84, 1.19\}$
GW230529	3.5	1.4	0.40	12.3	9.82	Yes	5	$\{0, 0.73, 0.89\}$

gravitational wave observations of BHNS binaries to PN results for EsGB. In comparison, the largest coupling we consider for the GW200115-like event ($\lambda = 0.1 m_{\rm BH}^2$) corresponds to $\sqrt{\alpha_{\rm GB}} \sim 1.19$ km, which is at the limit of the observational bound. For the tidally disrupted event, where the mass of the black hole is smaller, the largest coupling ($\lambda = 0.15 m_{\rm BH}^2$) corresponds to $\sqrt{\alpha_{\rm GB}} \sim 0.89$ km, i.e. within the observational bounds. We summarize the parameters of the BHNS systems we consider in Table I.

C. Diagnostic quantities

We use many of the same diagnostics as in Refs. [60,62], which we briefly review here. We measure the scalar and gravitational radiation by extracting the scalar field ϕ and the Newman-Penrose scalar Ψ_4 on coordinate spheres at large radii ($r = 100M$ where M is the total mass). We decompose Ψ_4 and ϕ into their spin -2 and spin 0 spherical harmonic components. We use the average value of ϕ at large radius $r = 100M$ to calculate the scalar charge $Q_{\rm SF}$. We sometimes find it useful to consider the gravitational wave strain $h \equiv h_+ + i h_\times$ instead, related to Ψ_4 through $\Psi_4 = \ddot{h}$. We numerically integrate Ψ_4 using fixed frequency integration [107].

We track the apparent horizon associated with the black hole, and measure its area and associated angular momentum $J_{\rm BH}$. From this, we compute the black hole mass $m_{\rm BH}$ via the Christodoulou formula [108]. We also track the total fluid rest mass outside the black hole horizon

$$M_0 = \int \rho u^t \sqrt{-g} d^3x \tag{7}$$

where ρ is the rest-mass density and u^a is the four-velocity of the fluid.

D. Post-Newtonian theory

In this section, we summarize existing PN predictions for gravitational and scalar waveforms in EsGB gravity. We perform a comparison with our numerical waveforms in Sec. IV B. As pointed out in Ref. [38], the relative size of the leading scalar dipolar radiation to the leading tensor quadrupolar radiation is

$$\frac{\mathcal{F}_{\rm nd}}{\mathcal{F}_{\rm d}} = \frac{24x}{5\zeta \mathcal{S}_-^2} \tag{8}$$

with $\mathcal{F}$ denoting the energy flux rate and the subscripts d and nd denoting the dipolar and nondipolar part of the energy flux rate, respectively. $x = (G_{\rm AB} M\Omega)^{\frac{2}{3}}$ is the PN expansion parameter (see, e.g., Refs. [38,109]) where $G_{\rm AB} = G(1 + \alpha_A \alpha_B)$ is the effective gravitational constant and $\alpha_{A/B}$ is the scalar charge of body A(B), and the gravitational constant is reintroduced for clarity. Finally, Ω is the orbital frequency, which we approximate as half the gravitational wave frequency [110–112]. In addition, ζ and $\mathcal{S}_-$ are PN parameters that depend on theory considered and are summarized in Table I of Ref. [109]. For the range of frequencies and coupling values we probe in our simulations, we find that the quadrupolar radiation dominates over the dipolar radiation by a factor of ∼40–100, meaning we are in the so-called *quadrupole driven regime* [38].

We first consider the gravitational modes $h_{\ell m}$ whose PN expression have been computed to 2PN[6] order in scalar-tensor theories [38] and, more recently, to 1PN directly in EsGB [57,58]. We consider the PN expressions from Ref. [38]

$$\frac{r}{M} h_{\ell m} = 2\tilde{G}(1-\zeta)\eta x \sqrt{\frac{16\pi}{5}} \hat{H}_{\ell m} e^{-im\psi}, \tag{9}$$

where $\eta = m_{\rm BH} m_{\rm NS}/M^2$ is the symmetric mass ratio, ψ the orbital phase given by Eqs. (60), (61) of Ref. [38], and $\tilde{G}$[7] is a PN parameter again defined in Table I of [109]. The expressions for the amplitude modes $\hat{H}_{\ell m}$ are long, and given in Eq. (67) of Ref. [38]. We have mapped these expressions to EsGB using the mapping outlined in Sec. IV A of Ref. [114]. Note that, tidal effects, which enter into the

[6]We adopt the convention that all PN order are relative to the quadrupolar radiation in GR. In this convention, the dipolar radiation enters at -0.5PN in the waveform and -1PN in the energy flux [113].

[7]Comparing with Eq. (65) of [38] we note that we have replaced G with $\tilde{G}$ to avoid confusion with our gravitational constant G. $\tilde{G}$ is the notation used in Ref. [113] and Table I of Ref. [109].

phase evolution at 5PN [115], were ignored in Ref. [38]. This is a reasonable assumption here, since after using the values listed in first row of Table I we find that the mass-weighted tidal deformability $\tilde{\Lambda}^{\rm GR} \sim 13$ of the system is small, and hence is expected to have little impact on the binary dynamics. We also note that scalar-induced dipolar tidal effects derived to leading order for nonspinning binary black holes in EsGB [116], and to next-to-next-to-leading order in scalar-tensor theories [117], vanish for shift-symmetric EsGB gravity.

We next consider the spherical harmonic components of the scalar radiation $\phi_{\ell m}$. These were derived to relative 0.5PN order in EsGB in Refs. [57,58], and relative 1.5PN order (2PN order beyond the leading dipolar contribution in waveform) in scalar tensor theories by Ref. [113]. Here, we use the results of Ref. [113] and map them to EsGB using the mapping of Sec. IV.B of Ref. [114], keeping only leading order terms in $\lambda/m_{\rm BH}^2$. The expressions can be found in Appendix E of Ref. [114].[8]

IV. RESULTS

We follow the evolution of two types of BHNS binaries distinguished by whether the neutron star is tidally disrupted before merger (see Table I). For both scenarios, we vary the EsGB coupling all the way up to near the maximum value for which we were able to carry out the evolution. We first consider a system with GW200115-like parameters and evolve it both in GR and EsGB gravity with a coupling comparable to the upper bound obtained in Ref. [45]. In Sec. IV A, we first focus on the dynamics during inspiral and show that the EsGB system inspiral faster than its GR counterpart. We then compare both the scalar and gravitational radiation to predictions from PN theory in Sec. IV B. Our main result is that the PN prediction is a good approximation to the amount of dephasing in binary up to late in the inspiral. In Sec. IV C, we focus on the merger dynamics and trends with varying EsGB coupling. We find a negligible change in amplitude of gravitational wave signal at merger. Independently of whether the neutron star is tidally disrupted, the main effect on the ringdown signal is not a shift in ringdown frequencies but a change in the amplitude of the signal. Specifically, the amplitude increases (or decreases) with increasing coupling when the neutron is (or is not) tidally disrupted. In the case where the neutron star is tidally disrupted, we also study the amount of material remaining outside the black hole after the merger and find a slight decrease in the amount of material leftover with increasing coupling due to the neutron star being more compact.

[8]Note that Ref. [114] uses different conventions from this paper so that, $\phi = \sqrt{2}\varphi$ where φ is scalar field in Ref. [114].

A. Comparison between GR and EsGB during inspiral

We first consider the BHNS system with GW200115-like parameters and an initial separation of $D = 10.35M$. We evolve the system both in GR and with a coupling value of $\sqrt{\alpha_{\rm GB}} = 1.19$ km. For the parameters and EOS we consider, the neutron star is swallowed by the black hole without tidal disruption (see the first row of Table I).

For simplicity, we use the same initial data for the EsGB system and its GR counterpart, i.e. we set $\phi = \partial_t \phi = 0$ on the initial time slice but slowly ramp on the coupling of the theory over $100M$. In the bottom panel of Fig. 1, we show the average value of the scalar field on the black hole apparent horizon. Note that the black hole acquires its scalar charge on a timescale much shorter than the inspiral timescale and we therefore do not expect our results after this transitory period to be noticeably affected. We have also checked that the scalarization process does not appreciably impact the orbital eccentricity or increase the level of constraint violation compared to that coming from truncation error (see Appendix).

The top panel of Fig. 1 shows the evolution of the coordinate separation between the two compact objects for the GR and EsGB systems. We first note that the merger part of both systems can be aligned through a time shift (see below). This implies they have a similar orbital separation or frequency for the onset of the plunge. This arises because the gravitational attraction in EsGB gravity is characterized by the effective gravitational constant $G_{\rm AB} = G(1 + \alpha_A \alpha_B)$ introduced earlier. Since the neutron star charge $\alpha_{\rm NS} = \mathcal{O}(\lambda^3)$ is negligible, the gravitational pull of a BHNS

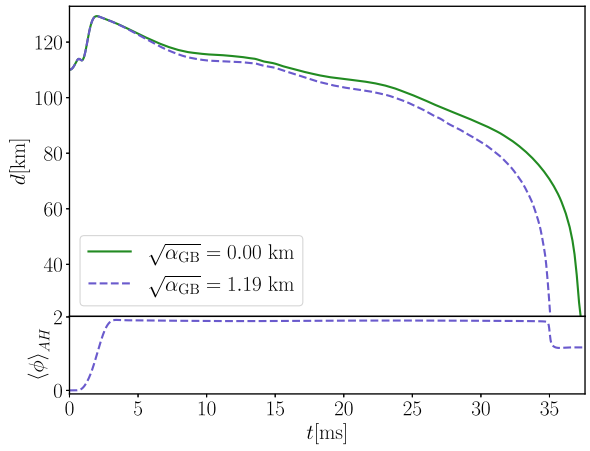

FIG. 1. (Top) Coordinate separation of BHNS merger with binary parameters consistent with the GW200115 event in GR and EsGB gravity with a coupling value of $\sqrt{\alpha_{\rm GB}} = 1.19$ km. With the chosen initial separation, the binary undergoes ~7 orbits before merger in GR. The increase in coordinate separation during the first 2 ms is due to the transition to damped harmonic gauge. The bottom panel shows the value of the scalar field averaged on the black hole apparent horizon for the EsGB case.

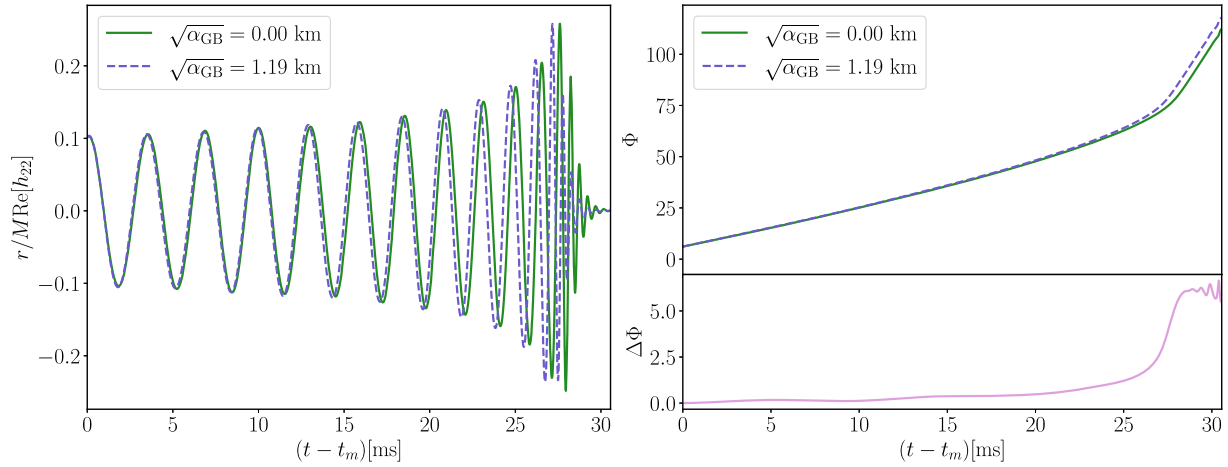

FIG. 2. Left: gravitational wave radiation for a BHNS merger with binary parameters consistent with the GW200115 event in GR and EsGB gravity with a coupling value of $\sqrt{\alpha_{\rm GB}} = 1.19$ km. We show the real part of the $\ell = m = 2$ spherical harmonic of the gravitational wave strain h extracted at $100M$. Right: the gravitational wave phase of the aligned waveforms Φ. The bottom shows the phase difference between the two waveforms $\Delta\Phi = \Phi_{\rm GB} - \Phi_{\rm GR}$. The waveforms have been aligned in time and phase at a gravitational wave frequency $f_m = 0.01/M$, or equivalently $t_m = \{9.7, 8.1\}$ ms for $\sqrt{\alpha_{\rm GB}} = \{0.0, 1.19\}$ km according to Eq. (10).

system in GR and EsGB is similar. By contrast, in binary black hole mergers, both black holes carry a positive scalar charge (see below for the explicit value), which increases the gravitational pull and therefore the orbital separation at which the objects merge. However, the BHNS system in EsGB still admits an additional energy dissipation channel via scalar radiation, and hence inspirals faster compared to GR, as can be seen from Fig. 1.

The shorter inspiral in EsGB gravity also leads to a shorter gravitational wave signal. Figure 2 shows the $\ell = m = 2$ harmonic of the strain in GR and EsGB. We align the two waveforms by requiring that the EsGB and GR waveform agree in time and phase at some fiducial frequency ω_m. More precisely, we leave the GR waveform untouched but construct a new shifted EsGB waveform

$$h_{22}^{\rm GB\prime}(t) = h_{22}^{\rm GB}(t + t_c - t_m) e^{i(\Phi_{\rm GB}(t_c) - \Phi_{\rm GR}(t_m))}, \quad (10)$$

where t_c is the time so that the derivative of the complex phase of EsGB waveform satisfies $\dot{\Phi}_{\rm GB}(t_c) = \omega_m$ and similarly t_m is the time where $\dot{\Phi}_{\rm GR}(t_m) = \omega_m$. Note that the gravitational wave frequency computed from the time derivative of the complex phase of the numerical waveform is typically noisy at early times and becomes smoother near the merger. To allow a matching at any time, we fit a polynomial in time through the frequency. In Fig. 2, $Mf_m = M\omega_m/(2\pi)$ was chosen to be 0.01. We also show the phase evolution Φ of the aligned waveforms in the right panel of Fig. 2, as well as the corresponding waveform phase differences,

$$\Delta\Phi = \Phi_{\rm GB} - \Phi_{\rm GR} \quad (11)$$

in the bottom right panel of Fig. 2. After the amplitude of the EsGB waveform peaks, it takes the GR waveform another ~4.3 radians to peak. Similarly to the binary black hole mergers in Ref. [62], we find that the dominant truncation error in our simulations does not depend strongly on the value of the coupling and therefore partially cancels out when calculating the difference in gravitational wave phase between EsGB and GR simulations using the same resolution. See Appendix for details. We estimate the truncation error in $\Delta\Phi$ to be ~1.2. This is smaller than the estimated phase error in the GR waveform itself.

B. Comparison to post-Newtonian theory

We now quantitatively compare the gravitational and scalar waveforms we obtain from our numerical evolution with the existing PN predictions in EsGB gravity outlined in Sec. III D. Along the way, we comment on the accuracy of current methods using PN predictions to constrain EsGB gravity.

Considering the same system as in the previous section, we use Eq. (9) to compute the PN prediction for dephasing of gravitational wave phase,

$$\Delta\Phi_{\rm PN} = 2\Delta\psi = 2(\psi_{\rm GB} - \psi_{\rm GR}) \quad (12)$$

and compare this to the dephasing in our numerical simulation, $\Delta\Phi_{\rm NR}$ [see Eq. (11) and Fig. 2]. Similarly we also compare the relative change in amplitude of waveform,

$$\frac{\Delta A}{A} = \frac{|h_{22}^{\rm GB}| - |h_{22}^{\rm GR}|}{|h_{22}^{\rm GR}|} \quad (13)$$

computed using Eq. (9) and in our numerical simulation. In Fig. 3, we show the numerical and PN prediction for the relative change in amplitude and dephasing as a function of gravitational wave frequency. We note that, as was mentioned

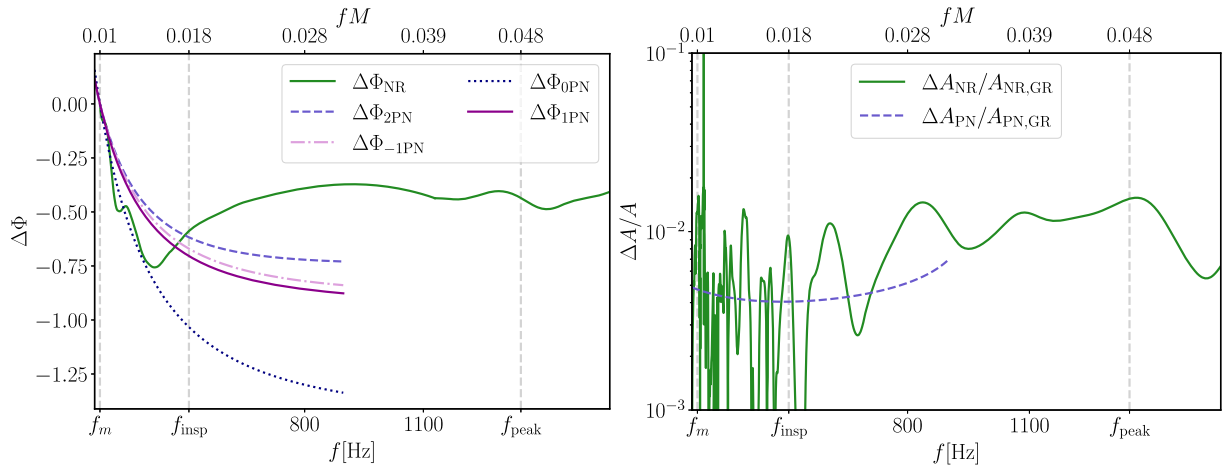

FIG. 3. PN and numerical predictions for the dephasing (left) and correction to the amplitude (right) of gravitational waveform of the binary shown in Fig. 2 [see Eqs. (11)–(13)]. We also show the dephasing when only considering leading order (dipolar) contribution to phase and all contributions up to 0PN and 1PN order. The first vertical line corresponds to frequency at which waveforms are aligned f_m according to Eq. (10), the second line to the end of inspiral stage in GR $f_{\rm insp}$, and the third to frequency at which amplitude of GR waveform peaks $f_{\rm peak}$.

in the previous section, although the binary in EsGB inspirals faster than in GR, the frequency at which the objects merge is similar, with an agreement of ∼2% for this particular system. More precisely, the left panel shows the total dephasing computed to 2PN, $\Delta\Phi_{\rm 2PN}$, but also when considering the leading dipolar (-1PN) contribution only, $\Delta\Phi_{\rm -1PN}$, as well as the dephasing computed up to 0PN and 1PN (we omit the 0.5PN and 1.5PN results for clarity). Since the EsGB corrections to the waveform within the PN expansions are only expected to be valid during the inspiral stage, tests of GR on the inspiral turn off corrections to GR at some cutoff frequency, which was taken to be $f = 0.018/M$ (or ∼500 Hz for this particular system) in Ref. [45].[9] We find that the difference between the PN and numerical results up to $f = 0.018/M$ are smaller than or comparable to our estimates of the truncation error in $\Delta\Phi$. Our result suggests that using the PN expansion up to $f = 0.018/M$ to constrain EsGB gravity, as was done in Ref. [45], is a good approximation.

A similar argument would apply to constraints that would be obtained by mapping constraints on the -1PN coefficient (from a parametrized test) to constraints on $\sqrt{\alpha_{\rm GB}}$ through the post-Einsteinian formalism [118], as was done in, for instance, Refs. [7,52]. It would be interesting to perform parameter estimation on our numerical simulations using not only the PN results for EsGB, as was done for the observational data in Refs. [45,51]; but also using theory-agnostic approaches, such as the TIGER [48,49] or FTI [50] frameworks, which constrain the PN coefficients by varying them one at a time. However, this is beyond the scope of this paper, and we leave it to future work. Note that the left panel of Fig. 3 also shows that the leading order dipolar contribution to the dephasing dominates. Although a more detailed study would be required, this indicates that constraints on the leading PN coefficient recovered when only variations at that particular order are allowed (as is typically done in most current analyses), would in the case of EsGB, be a satisfactory assumption, which was already argued in Ref. [119].

We note that the PN prediction combining all orders predicts that the EsGB system should inspiral faster than GR at any given frequency all the way up to near merger, but that this effect diminishes at high frequencies. Moreover, we find that the highest PN corrections, namely 1.5 and 2PN (see Fig. 3), reduce the rate of inspiral with respect to GR. This trend is consistent with our numerical simulations which show in Fig. 3 that the extra dephasing past the inspiral stage is negligible. This is in agreement with Ref. [109], where it was found that when considering the conservative part of the dynamics, including higher PN orders tends to decrease the orbital frequency of the binary at the innermost stable circular orbit. This further suggests that setting the corrections to the phase to zero past the inspiral stage, as in Refs. [45,51,52] is a good approximation, at least for EsGB gravity where we find that the changes to the phase during merger and ringdown are small.

Finally, we note that the PN prediction for the amplitude of waveform, shown in right panel of Fig. 3, is consistent with our numerical results, and that the relative change in amplitude of waveform remains small throughout the inspiral. This further motivates generic inspiral tests of GR on the phase rather than the amplitude of waveform.

[9]Parametric tests on the inspiral done in the LVK analyses in Refs. [9–12,15] use a cutoff frequency of $f_c^{\rm PAR} = 0.35 f_{\rm peak}^{22}$ where $f_{\rm peak}^{22}$ is the GW frequency at the peak amplitude of ($\ell = 2$, $m = 2$) waveform. In our particular setup, this would correspond to a frequency of $fM \sim 0.017$.

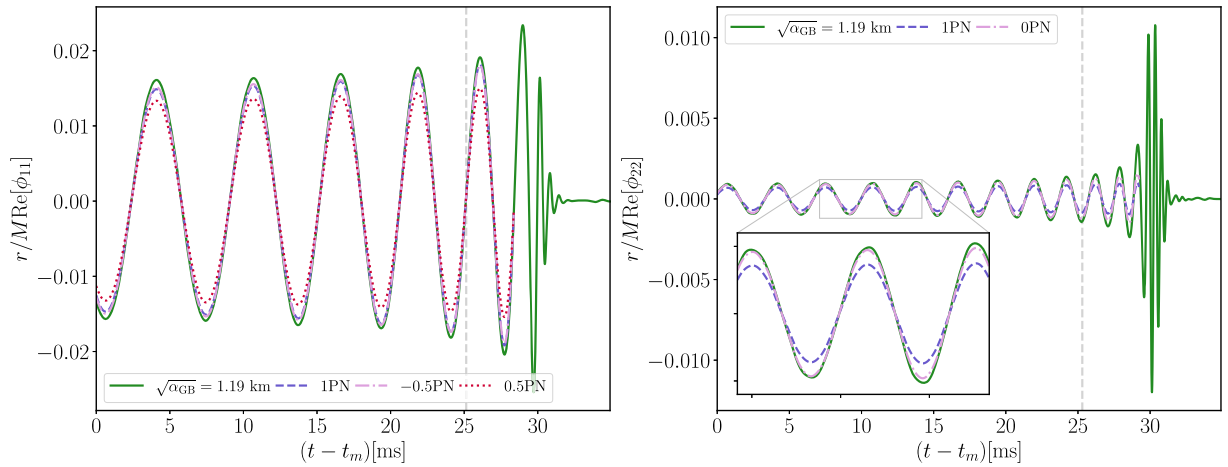

FIG. 4. Scalar radiation for a BHNS binary merger with binary parameters consistent with the GW200115 event for a coupling value of $\sqrt{\alpha_{\rm GB}}=1.19$ km. We show the real part of the $(\ell=2,m=2)$ (right) and $(\ell=1,m=1)$ (left) spherical harmonic of scalar waveform ϕ extracted at $100M$. During the inspiral, we also display the PN predictions derived to relative 1.5PN. The vertical line roughly corresponds to time at which modifications to GR are turned off in Ref. [45], i.e. $t(f_{\rm insp}=0.018/M)$. Time is measured with respect to time where both waveforms have a gravitational wave frequency $f_m=0.01/M$.

We next compare the spherical harmonic components of the scalar radiation $\phi_{\ell m}$ extracted from our simulations with PN predictions. In Fig. 4, we compare our numerical scalar modes ϕ_{11} and ϕ_{22} to the PN predictions at successively higher PN orders. As in the comparisons of scalar waveforms computed in Refs. [57,58,62,65], the frequency we use in the PN expressions are obtained from our numerical evolutions, so our comparison is measuring the accuracy of the PN approximation in determining the amplitude of the scalar field, given its frequency. We see that the lowest PN order contributes the most to the amplitude of waveform. We find that the fractional difference between the numerical waveforms and the 1PN $(\ell=1,m=1)$ mode is about 5%, while for the $(\ell=2,m=2)$ it is initially ∼22% and grows as binary inspirals. We note that the inclusion of the next-to-leading order in the $(\ell=2,m=2)$ waveform worsens the agreement between the PN and numerical waveform, so higher PN terms may be needed for better agreement with numerical simulations.

C. Merger dynamics and trends with varying EsGB coupling

Lastly, we study the effects of EsGB on the merger and ringdown of two different scenarios: a BHNS merger with the same intrinsic parameters as in the previous two sections, i.e. GW200115-like, but with smaller initial separation and considering additional values for the

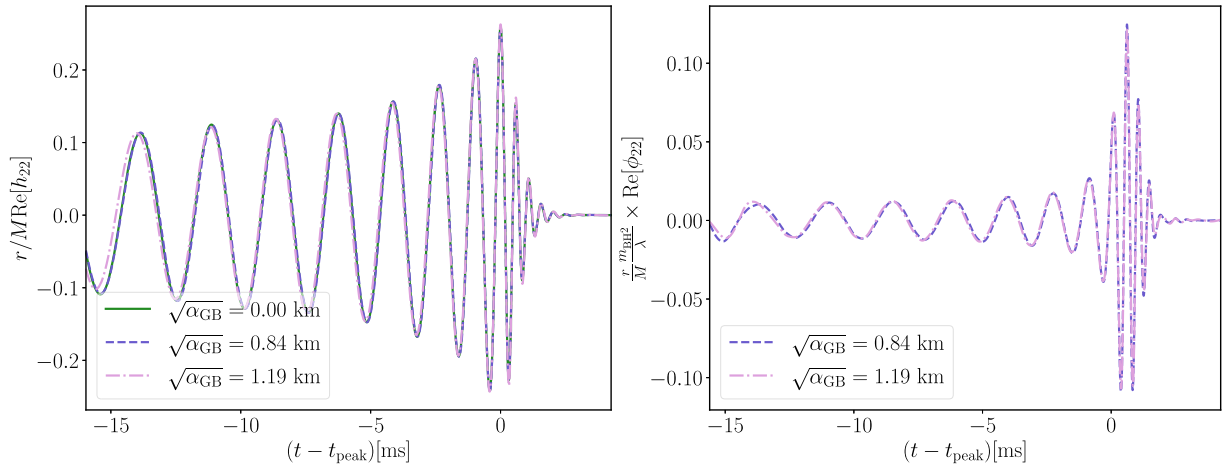

FIG. 5. Gravitational wave radiation (left) and scalar radiation (right) for a BHNS merger with binary parameters consistent with the GW200115 event for different values of the EsGB coupling. We show the real part of the $(\ell=2,m=2)$ spherical harmonic of the strain h and (2,2) component of ϕ both extracted at $100M$. Time is measured with respect to the time where amplitude of h_{22} is maximum $t_{\rm peak}$.

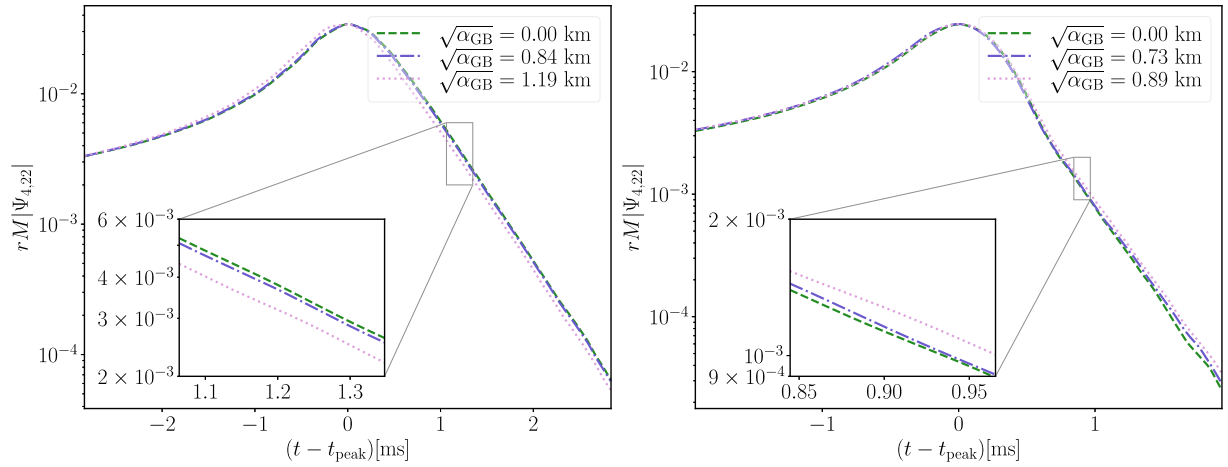

FIG. 6. The amplitude of the $\ell = 2$, $m = 2$ spherical harmonic Ψ_4 for a BHNS binary merger with parameters consistent with the GW200115 event (left) and for a binary where the neutron star is tidally disrupted (right) for different values of the EsGB coupling. Time is measured with respect to $t_{\rm peak}$, the time where $|\Psi_{4,22}|$ is maximum.

coupling, and a GW230529-like BHNS merger where the neutron is tidally disrupted before merger (see Table I). For these two systems, we vary the EsGB coupling up to near the maximum value where we are able to carry out the evolution, allowing us to study the trends with the coupling of the theory.

Figure 5 shows the gravitational (left) and scalar radiation (right) for the first scenario. After ~ 4–5 orbits, the black hole swallows the neutron star and rings down to form a final remnant black hole with a larger mass. In addition to GR, we consider two other couplings, $\sqrt{\alpha_{\rm GB}} = 0.84$ km and 1.19 km, with the largest value at the limit of the observational bounds, $\sqrt{\alpha_{\rm GB}} \sim 1.19$ km. Here we align the waveforms in time and phase at the peak of amplitude of the gravitational waveforms. Despite the shorter inspiral, we observe some dephasing in the $\ell = 2$, $m = 2$ harmonic of the strain (left panel), consistent with EsGB binaries merging faster the larger their coupling due to the additional energy loss through scalar radiation. The $\ell = 2$, $m = 2$ component of the scalar radiation (right panel) shows similar behavior to the gravitational waves both in the inspiral and ringdown. After rescaling for the test-field dependence on coupling, we find that there is a mild nonlinear enhancement just before merger, but this is negligible earlier in the inspiral and during ringdown.

The gravitational quasinormal modes of rotating black holes were computed numerically in Ref. [106] by performing a slow-rotation expansion, as in Ref. [105], to second order in the dimensionless spin parameter $a \equiv J/m_{\rm BH}^2$ (where J is the angular momentum of black hole).[10] According to Ref. [106], the real frequency of the fundamental $\ell = 2$, $m = 2$ quasi-normal mode of a black hole in EsGB gravity should decrease with coupling and the relative change should be $\sim 1\%$ for the largest coupling we consider here. The correction to the decay rate (imaginary frequency) changes from a positive to a negative correction for the values of spins and couplings we probe and is expected to be negligible. We note that Ref. [106] found that the expansion in λ/m_f^2, where m_f is mass of remnant black hole, is accurate within 1% as long as $\lambda/m_f^2 < 0.07$ for the real modes and $\lambda/m_f^2 < 0.053$ for the imaginary modes. The couplings we consider correspond to $\lambda = 0.032 m_f^2$ and $0.066 m_f^2$, meaning the results here should be applied with care.[11] We find that the real frequency decreases with increasing coupling and that the relative change is on the order of $\sim 1\%$ for the largest coupling considered, i.e. it is the right order of magnitude, but it is too small to reliably quantify with our current numerical data. The change in the imaginary part is negligible, also in agreement with perturbation theory. The most noticeable effect is a suppression in the amplitude of ringdown gravitational wave signal with increasing coupling as shown in the left panel of Fig. 6 (by $\approx 10\%$ for the largest coupling), which is consistent with an increasing amount of radiation going into the scalar field with increasing coupling.

[10]We note that more recently Ref. [120] developed a general method using perturbative spectral expansions to compute quasinormal modes in a wide class of modified theories of gravity for black holes of any sub-extremal spin and applied this method to EsGB gravity.

[11]We also note that Ref. [106] argued that, although the results are only accurate to second order in spin, with an appropriate resummation of the spin expansion parameter, the results should be accurate for dimensionless spins as large as ~ 0.7. The results quoted here were obtained using the fitting formula Eq. (47) in Ref. [106] which do not include the resummation. Note also that the computation of the quasinormal modes in Refs. [104–106] were performed in Einstein-dilaton-Gauss-Bonnet gravity, which is equivalent to the EsGB gravity theory considered in this work only in the limit where ϕ is small.

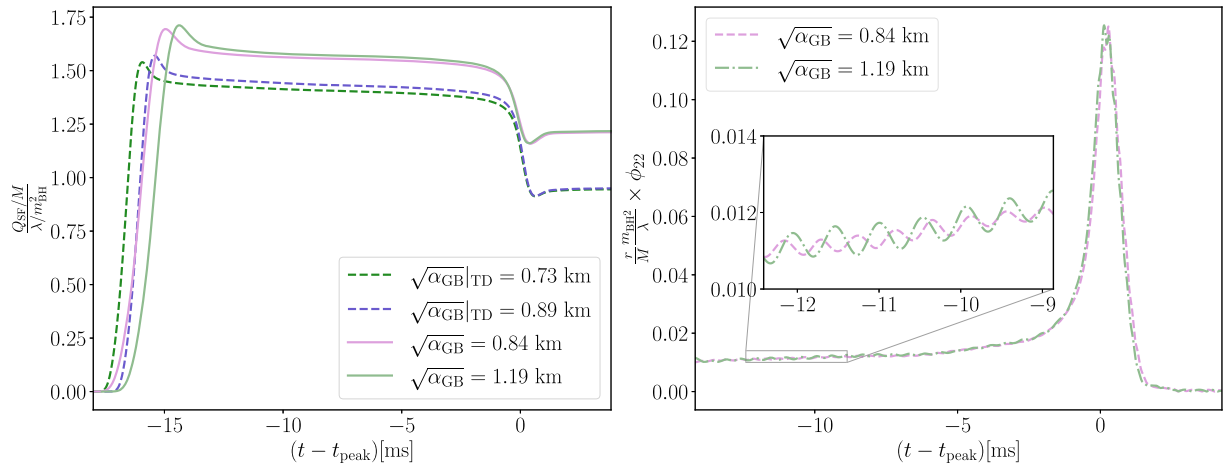

FIG. 7. Left: the scalar charge $Q_{\rm SF}$ rescaled by $\lambda/m_{\rm BH}^2$, measured from the average value of the scalar field at $100M$ as a function of retarded time $(t-r)/M$, for the BHNS mergers considered in this paper (see the last two rows of Table I). The mergers where the neutron star is tidally disrupted (TD) are indicated by dashed lines. Right: amplitude of scalar radiation for a BHNS merger with binary parameters consistent with the GW200115 event for different values of the EsGB coupling. We show the amplitude of the ($\ell = 2$, $m = 2$) component of ϕ extracted at $100M$. Time is measured with respect to when $|\Psi_{4,22}|$ is maximum.

The amplitude of the $\ell = 2$, $m = 2$ mode of the scalar waves, shown in Fig. 7, displays small, yet measurable, oscillations that track the neutron star oscillations in the fundamental fluid mode (f-mode) of the star. These are evident in the oscillations of the star's central value of both the rest mass density and the scalar field value $\phi_{\rm c}$ (see Fig. 8). The relative amplitude of the oscillations in the central density are not strongly affected by the value of the GB coupling and hence do not seemed to be an artifact of the way we turn on the scalar field. Instead, we attribute the oscillations to numerical errors as they decrease as the numerical resolution is increased. Finally, we note that the right panel of Fig. 8 shows that turning on the EsGB coupling increases the central density of neutron star, up to 10% for the largest coupling we consider, as predicted from numerical studies of single neutron stars in EsGB [73].

We also consider a BHNS merger where the neutron is tidally disrupted before merger, with binary parameters similar to the GW230529 event(see last row of Table I). We show the gravitational and scalar radiation in Fig. 9. The binary here undergoes ∼5 orbits before merger. We consider evolutions with coupling values of $\sqrt{\alpha_{\rm GB}} \sim 0.73$ and 0.89 km, where the highest coupling is 50% larger, when normalized by the black hole mass, than considered in the previous case. Similarly to before, we find that the most noticeable effect is the decrease in the inspiral timescale with increasing coupling. According to perturbation theory, the larger the dimensionless coupling value λ/m_f^2 and spin of remnant black hole, the larger the change in real and imaginary frequencies of quasinormal modes. In comparison to the previous case, the final remnant here is smaller,

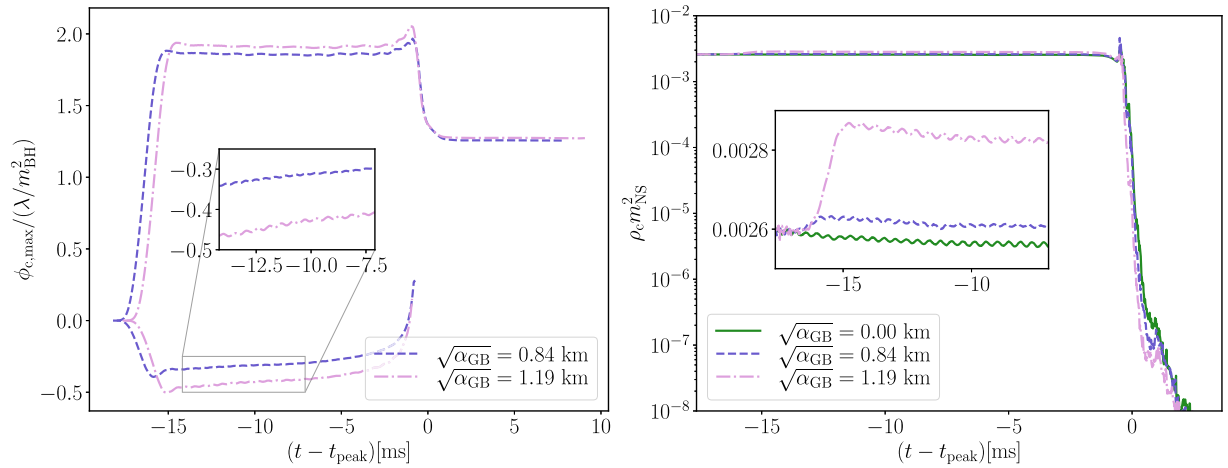

FIG. 8. Left: The maximum value of the scalar field over the numerical domain (excluding black hole interior) and value of the scalar field at the center of the neutron star (which is negative for most of the evolution). Right: The maximum rest-mass density (located at center neutron star). These results are for the GW200115-like BHNS merger and various EsGB coupling values.

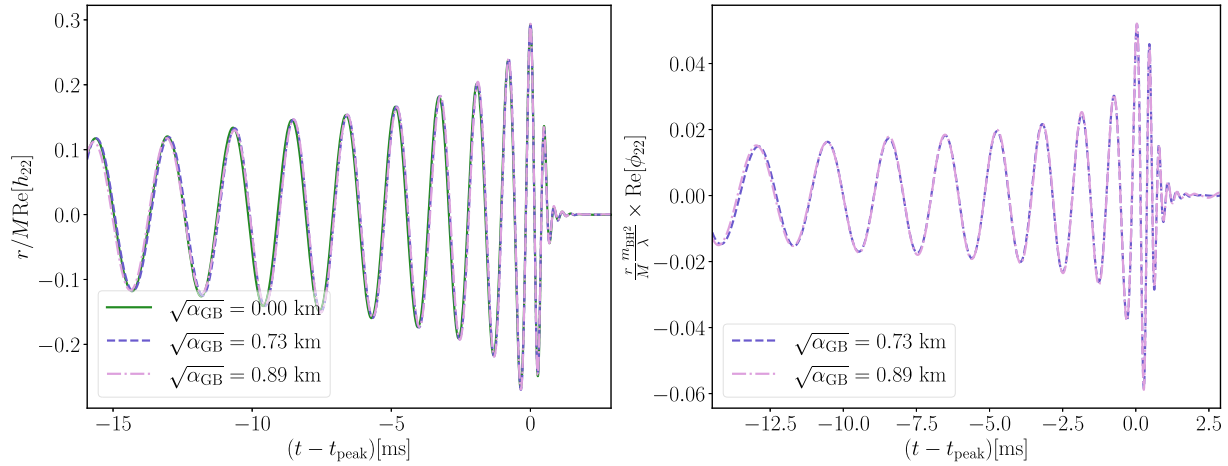

FIG. 9. Gravitational wave radiation (left) and scalar radiation (right) for a BHNS merger where the neutron star is tidally disrupted for different values of the EsGB coupling. We show the real part of the $(\ell, m) = (2, 2)$ spherical harmonic of the strain h and (2,2) component of ϕ both extracted at $100M$. Time is measured with respect to the time where $|h_{22}|$ is maximum.

leading to higher coupling values of $\lambda = 0.054m_f^2$ and $0.082m_f^2$, and the final dimensionless spin is $\sim$0.6, while it was previously 0.5. Both of these effects lead to a larger change in the quasinormal frequency, with a predicted relative change in the real frequency of -2% for the largest coupling we consider and a change of -0.65% for the decay rate, according to Ref. [106] (and with the caveats discussed above). Although we find that the change in the real frequency has the right order of magnitude and the change in imaginary frequency has the right sign, they are both still too small to reliably quantify.

The main difference compared to the binary where the neutron star is not tidally disrupted is that the amplitude of the ringdown gravitational wave signal increases slightly with increasing coupling (by $\approx$2% for the largest coupling), as shown in the right panel of Fig. 6. We hypothesize that this can be attributed to the fact that the neutron star is more compact, and less strongly tidally disrupted for larger couplings. Consistent with this, we also find a small increase in the amount of fluid rest mass falling into the black hole with increasing coupling, as shown in Fig. 10. We find that the amount of mass remaining outside of the black hole 8 ms after merger decreases from a value of $0.049M_\odot$ in GR to $0.047M_\odot$ for the largest coupling we considered (3.5% decrease). Of this postmerger material, we estimate that $\sim 10^{-3}M_\odot$ is gravitationally unbound from the system with mildly relativistic asymptotic velocities; we find no clear trend in the unbound material with EsGB coupling values. In passing, we note that the leftover rest mass in GR is roughly an order of magnitude larger than that predicted by the fitting formula in Ref. [121]. Though some of the discrepancy may be due to truncation error, the formula in Ref. [121] was also not fit with any simulation results in the range $q^{-1} \in (1.2, 3)$, making it difficult to judge its uncertainty in this regime.

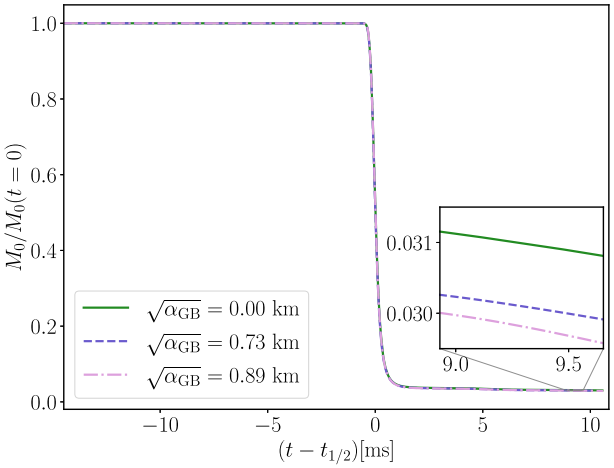

FIG. 10. The total fluid rest mass outside black hole horizon for the merger where the neutron star is tidally disrupted for different values of the EsGB coupling. Time is measured with respect to the time where half of the neutron star mass has been accreted onto black hole $t_{1/2}$ and the rest mass is normalized by its initial value.

V. DISCUSSION AND CONCLUSION

In this work, we have taken advantage of recent advances in solving the full equations of EsGB gravity to study BHNS mergers for the first time. This was motivated by the fact that neutron stars do not have scalar charge in this theory and black hole masses in such binaries are typically small in comparison to binary black holes [122], making them an ideal probe to test for modifications to GR at smaller curvatures length scales. We find that the BHNS binaries inspiral faster in EsGB relative to GR due to the emission of scalar radiation. We first evolved a system chosen to be consistent with GW200115 and with EsGB coupling at the limit of the observational bounds placed by applying PN predictions to the event. Comparing our scalar

and gravitational waveforms to existing PN predictions for EsGB, we find reasonable agreement in the dephasing relative to GR all the way up to end of ∼500 Hz, in part due to the fact that the dephasing between GR and EsGB becomes small in the final orbits. This suggests current bounds on EsGB using PN theory up to the end of inspiral phase are a good approximation. It would be interesting to carry out a full Bayesian parameter estimation using PN theory as well as the theory agnostics approaches such as TIGER or FTI to better understand how these methods perform and study some of the degeneracies that might arise and lead to parameter estimation biases. To fully understand the observational prospects of constraining EsGB gravity with BHNS mergers, future work should also explore a range of EOSs, EsGB couplings, and binary parameters, and understand possible degeneracies, including with tidal effects [39].

In addition to measuring the dephasing, we also found that the leading order PN contribution compares well in matching the amplitude of scalar radiation emitted during the inspiral at a given frequency. This is in qualitative agreement with binary black hole simulations in EsGB [62], and can be partially explained by the fact that corrections to the scalar field amplitude in the GB coupling enter at third order for shift-symmetric EsGB gravity (see, e.g., Appendix D of [62]). We also note that the next-to-leading order was found to increase the error in amplitude, and the next-to-next-to-leading order is needed to improve consistency.

We also studied the effect of modifications to GR on the dynamics of the merger and ringdown signal of newly formed black hole for two different scenarios: a BHNS merger where the neutron star is not tidally disrupted, and one where it is. Most of the literature has focused on computing a change in frequency using perturbation theory. However, for both cases considered here, we find that the frequency shift is small, in qualitative agreement with perturbative predictions, and we find that the dominant effect is instead a change in the amplitude of the ringdown signal. This observation is in agreement with evolutions of binary black hole and binary neutron star mergers in EsGB [59,62,123]. This observational signature could potentially be leveraged in ringdown tests of GR, but also introduces further complications [124–129]. In particular, we found a suppression of the amplitude with increasing coupling when the neutron star is not tidally disrupted, explained by an increase by the amount of emitted scalar radiation. However, when the neutron star is tidally disrupted, we found that the amplitude increases with coupling, which we attribute to the fact that, for a fixed EOS, the NS is more compact and less easily tidally disrupted.

Even setting aside modified gravity considerations, the lower mass ratio case we consider ($q = 0.4$) probes a regime that has not been extensively studied using full GR simulations of BHNS mergers, but has become particularly interesting with the observation of GW230529. It is worth noting that we find (in GR) that an accretion disk forms postmerger with a few percent of a solar mass, which is one order of magnitude larger than the prediction of the commonly used fitting formula in Ref. [121] for this particular case. Coupled with other recent studies [130,131], this suggests that analyses using this formula may underestimate the prospects for a postmerger electromagnetic transient in this part of the parameter space.

Though not comprehensively addressed here, it would also be interesting for future work to quantify how modified gravity affects potential electromagnetic transient arising from the merger. This would involve considering a range of binary parameters and choices for the neutron star EOS in order to determine under what circumstances modified gravity effects could be important, and nondegenerate with other parameters, in determining the size of the postmerger accretion disk, the amount of unbound material, and other properties that affect potential electromagnetic signatures.

ACKNOWLEDGMENTS

We thank Erik Schnetter and Samuel Toothe for their assistance constructing the initial data used here. M. C. is grateful to Harald Pfeiffer and Elise Sänger for helpful discussions regarding various aspects of this project. M. C. is especially thankful to Félix-Louis Julié for sharing his notebook on how to transform the scalar field from the Jordan to the Einstein frame as well as answering various questions regarding PN calculations in EsGB gravity. We thank Michalis Agathos for reviewing this manuscript. W. E. acknowledges support from a Natural Sciences and Engineering Research Council of Canada Discovery Grant and an Ontario Ministry of Colleges and Universities Early Researcher Award. This research was supported in part by Perimeter Institute for Theoretical Physics. Research at Perimeter Institute is supported in part by the Government of Canada through the Department of Innovation, Science and Economic Development and by the Province of Ontario through the Ministry of Colleges and Universities. This research was enabled in part by support provided by SciNet [132] and the Digital Research Alliance of Canada [133]. Calculations were performed on the Symmetry cluster at Perimeter Institute, the Niagara cluster at the University of Toronto, and the Narval cluster at Ecole de technologie supérieure in Montreal. Computations were also performed on the Urania HPC system at the Max Planck Computing and Data Facility. This material is based upon work supported by NSF's LIGO Laboratory which is a major facility fully funded by the National Science Foundation.

APPENDIX: NUMERICAL CONVERGENCE AND ERROR ESTIMATES

For the BHNS mergers considered in this paper, we perform simulations with seven levels of refinement where

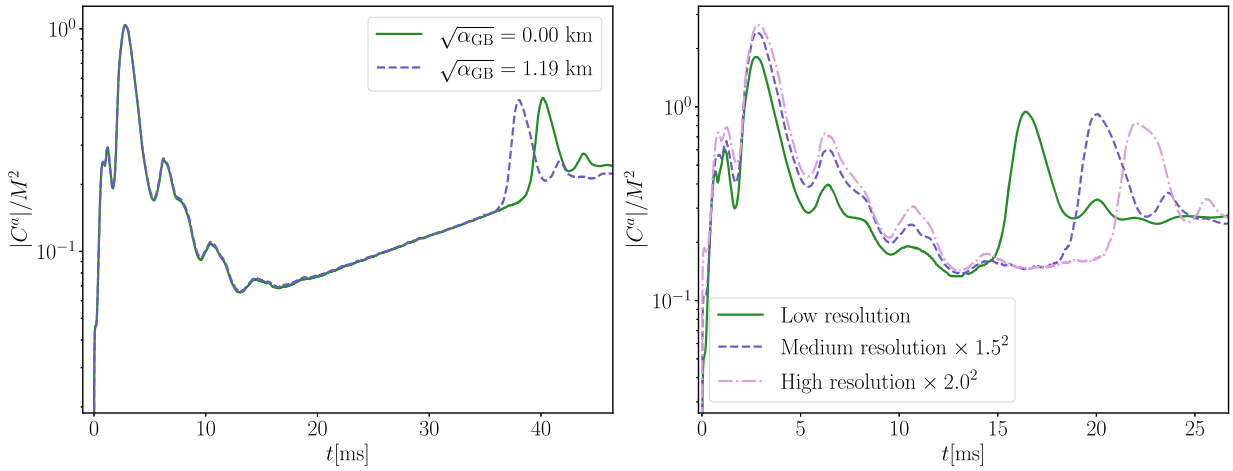

FIG. 11. Left: volume integrated norm of the modified generalized harmonic constraint violation C^a as a function of time for the BHNS system with GW200115-like parameters and an initial separation of $D = 9.8M$ in GR and EsGB with $\lambda = 0.1 m_{\rm BH}^2$. We observe that the constraints are the same modulo a time shift. Right: convergence of the volume integrated constraint violation for same system as in left panel, but for an initial separation of $D = 8.6M$ and at three resolutions. The values have been scaled assuming second order convergence, though at early times the convergence is closer to first order.

the finest level has a linear grid spacing of $dx \sim 0.016M$, and each successive level has a linear grid spacing that is twice as coarse. In Fig. 11, we show the norm of the modified generalized harmonic constraint violation, integrated over the domain as a function of time. In the left panel, we compare a simulation that transitions to a nonzero EsGB coupling to the equivalent simulation in GR. As can be seen, this transition does not noticeably impact the constraint violation, modulo the faster inspiral of the modified gravity system.

For the GW200115-like binary where the initial separation is $D = 8.6M$, we also perform a convergence study with grid spacing that is $4/3$ and $2/3\times$ as large, which is shown in right panel of Fig. 11. All results in the main text are from the medium resolution. Although at early times the order of convergence is closer to first order, presumably from high frequency noise (junk radiation) in the initial data which may engage the shock capturing scheme, at later times the convergence is consistent with roughly second order, as expected from our numerical scheme in the absence of shocks. In addition, we note that the constraints jump again at the end, which corresponds to when the NS starts to plunge into the BH.

We compare the dephasing between the EsGB and GR waveforms in Fig. 2 to the numerical errors in the simulations using the techniques applied to binary black

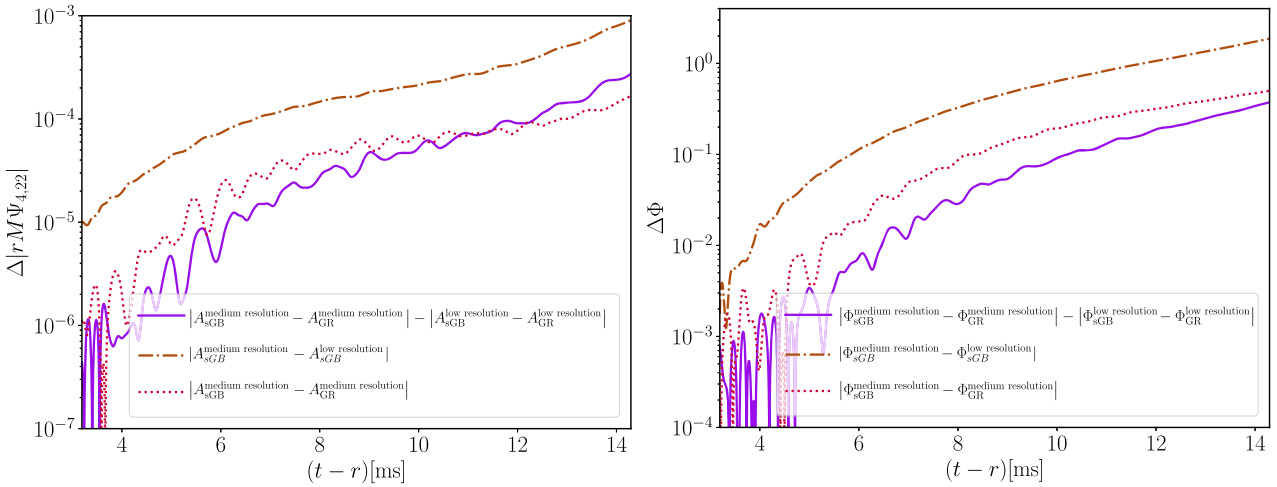

FIG. 12. We show the difference between the low and medium resolutions of the amplitude (left) and phase (right) of the gravitational waveform for the BHNS binary with GW200115 like parameters, an initial separation of $D = 8.61M$, and coupling of $\sqrt{\alpha_{\rm GB}} = 1.19$ km. We also show the difference between the EsGB and GR amplitude and phase at low and medium resolutions (dashed brown line). This provides evidence that the truncation error roughly cancels between the EsGB and GR runs.

hole mergers in Ref. [62] (and detailed in Appendix A of that paper). The error in the Richardson extrapolated phase at the frequency where GR peaks is ∼7.2 radians, which is comparable to the dephasing. However, similarly to the binary black hole mergers in Ref. [62], we find that the dominant truncation error in our simulations does not depend strongly on the value of the coupling and therefore partially cancels out when calculating the difference in gravitational wave phase between EsGB and GR simulations using the same resolution. We see evidence that this is the case, for example, by comparing a measure of the truncation error in $\Delta\Phi$, computed by comparing the GW200115 simulation starting at a shorter initial separation in GR to an equivalent EsGB simulation with $\sqrt{\alpha_{\rm GB}} = 1.19$ km at two different resolutions, to an estimate of the overall truncation error in Φ for the same EsGB case. We find the former to be ∼6× smaller than the latter (see Fig. 12 in the Appendix).

[1] B. P. Abbott *et al.* (LIGO Scientific and Virgo Collaborations), Phys. Rev. X **6**, 041015 (2016); **8**, 039903(E) (2018).
[2] B. P. Abbott *et al.* (LIGO Scientific and Virgo Collaborations), Phys. Rev. X **9**, 031040 (2019).
[3] R. Abbott *et al.* (LIGO Scientific and Virgo Collaborations), Phys. Rev. X **11**, 021053 (2021).
[4] R. Abbott *et al.* (LIGO Scientific, VIRGO, and KAGRA Collaborations), Phys. Rev. X **13**, 041039 (2023).
[5] C. M. Will, Living Rev. Relativity **17**, 4 (2014).
[6] N. Yunes and X. Siemens, Living Rev. Relativity **16**, 9 (2013).
[7] N. Yunes, K. Yagi, and F. Pretorius, Phys. Rev. D **94**, 084002 (2016).
[8] E. Berti *et al.*, Classical Quantum Gravity **32**, 243001 (2015).
[9] B. P. Abbott *et al.* (LIGO Scientific and Virgo Collaborations), Phys. Rev. Lett. **123**, 011102 (2019).
[10] B. P. Abbott *et al.* (LIGO Scientific and Virgo Collaborations), Phys. Rev. D **100**, 104036 (2019).
[11] R. Abbott *et al.* (LIGO Scientific and Virgo Collaborations), Phys. Rev. D **103**, 122002 (2021).
[12] R. Abbott *et al.* (LIGO Scientific, VIRGO, and KAGRA Collaborations), arXiv:2112.06861.
[13] E. Berti, K. Yagi, and N. Yunes, Gen. Relativ. Gravit. **50**, 46 (2018).
[14] E. Berti, K. Yagi, H. Yang, and N. Yunes, Gen. Relativ. Gravit. **50**, 49 (2018).
[15] B. P. Abbott *et al.* (LIGO Scientific and Virgo Collaborations), Phys. Rev. Lett. **116**, 221101 (2016); **121**, 129902 (E) (2018).
[16] J. F. Donoghue, Phys. Rev. D **50**, 3874 (1994).
[17] C. Burgess, Living Rev. Relativity **7**, 5 (2004).
[18] G. W. Horndeski, Int. J. Theor. Phys. **10**, 363 (1974).
[19] S. Alexander and N. Yunes, Phys. Rep. **480**, 1 (2009).
[20] S. Endlich, V. Gorbenko, J. Huang, and L. Senatore, J. High Energy Phys. 09 (2017) 122.
[21] C. de Rham, J. Francfort, and J. Zhang, Phys. Rev. D **102**, 024079 (2020).
[22] P. Kanti, N. Mavromatos, J. Rizos, K. Tamvakis, and E. Winstanley, Phys. Rev. D **57**, 6255 (1998).
[23] N. Yunes and L. C. Stein, Phys. Rev. D **83**, 104002 (2011).
[24] T. P. Sotiriou and S.-Y. Zhou, Phys. Rev. Lett. **112**, 251102 (2014).
[25] T. P. Sotiriou and S.-Y. Zhou, Phys. Rev. D **90**, 124063 (2014).
[26] G. Antoniou, A. Bakopoulos, and P. Kanti, Phys. Rev. Lett. **120**, 131102 (2018).
[27] A. Papageorgiou, C. Park, and M. Park, Phys. Rev. D **106**, 084024 (2022).
[28] T. Damour and G. Esposito-Farese, Phys. Rev. Lett. **70**, 2220 (1993).
[29] T. Damour and G. Esposito-Farese, Classical Quantum Gravity **9**, 2093 (1992).
[30] D. Anderson and N. Yunes, Classical Quantum Gravity **36**, 165003 (2019).
[31] S. W. Hawking, Commun. Math. Phys. **25**, 167 (1972).
[32] T. P. Sotiriou and V. Faraoni, Phys. Rev. Lett. **108**, 081103 (2012).
[33] T. Damour and G. Esposito-Farese, Phys. Rev. D **54**, 1474 (1996).
[34] E. Barausse, C. Palenzuela, M. Ponce, and L. Lehner, Phys. Rev. D **87**, 081506 (2013).
[35] C. Palenzuela, E. Barausse, M. Ponce, and L. Lehner, Phys. Rev. D **89**, 044024 (2014).
[36] F. M. Ramazanoğlu and F. Pretorius, Phys. Rev. D **93**, 064005 (2016).
[37] K. Yagi, L. C. Stein, N. Yunes, and T. Tanaka, Phys. Rev. D **85**, 064022 (2012); **93**, 029902(E) (2016).
[38] N. Sennett, S. Marsat, and A. Buonanno, Phys. Rev. D **94**, 084003 (2016).
[39] S. Ma, V. Varma, L. C. Stein, F. Foucart, M. D. Duez, L. E. Kidder, H. P. Pfeiffer, and M. A. Scheel, Phys. Rev. D **107**, 124051 (2023).
[40] R. Abbott *et al.* (LIGO Scientific, KAGRA, and VIRGO Collaborations), Astrophys. J. Lett. **915**, L5 (2021).
[41] J. Aasi *et al.* (LIGO Scientific Collaboration), Classical Quantum Gravity **32**, 074001 (2015).
[42] F. Acernese *et al.* (VIRGO Collaboration), Classical Quantum Gravity **32**, 024001 (2015).
[43] K. Somiya (KAGRA Collaboration), Classical Quantum Gravity **29**, 124007 (2012).
[44] Y. Aso, Y. Michimura, K. Somiya, M. Ando, O. Miyakawa, T. Sekiguchi, D. Tatsumi, and H. Yamamoto (KAGRA Collaboration), Phys. Rev. D **88**, 043007 (2013).
[45] Z. Lyu, N. Jiang, and K. Yagi, Phys. Rev. D **105**, 064001 (2022).

[46] R. Abbott *et al.* (LIGO Scientific and Virgo Collaborations), Astrophys. J. Lett. **896**, L44 (2020).
[47] The LIGO Scientific, Virgo, and KAGRA Collaborations, Astrophys. J. Lett. **970**, L34 (2024).
[48] M. Agathos, W. Del Pozzo, T. G. F. Li, C. Van Den Broeck, J. Veitch, and S. Vitale, Phys. Rev. D **89**, 082001 (2014).
[49] J. Meidam *et al.*, Phys. Rev. D **97**, 044033 (2018).
[50] A. K. Mehta, A. Buonanno, R. Cotesta, A. Ghosh, N. Sennett, and J. Steinhoff, Phys. Rev. D **107**, 044020 (2023).
[51] B. Gao, S.-P. Tang, H.-T. Wang, J. Yan, and Y.-Z. Fan, Phys. Rev. D **110**, 044022 (2024).
[52] E. Sanger, S. Roy, O. Birnholtz, A. Buonanno, T. Dietrich, M. Haney, F. Julié, J. Steinhoff, and C. van den Broeck, arXiv:2406.03568.
[53] B. P. Abbott *et al.* (KAGRA, LIGO Scientific, and VIRGO Collaborations), Living Rev. Relativity **21**, 3 (2020).
[54] S. Hild *et al.*, Classical Quantum Gravity **28**, 094013 (2011).
[55] B. P. Abbott *et al.* (LIGO Scientific Collaboration), Classical Quantum Gravity **34**, 044001 (2017).
[56] F.-L. Julié and E. Berti, Phys. Rev. D **100**, 104061 (2019).
[57] B. Shiralilou, T. Hinderer, S. Nissanke, N. Ortiz, and H. Witek, Classical Quantum Gravity **39**, 035002 (2022).
[58] B. Shiralilou, T. Hinderer, S. Nissanke, N. Ortiz, and H. Witek, Phys. Rev. D **103**, L121503 (2021).
[59] W. E. East and F. Pretorius, Phys. Rev. D **106**, 104055 (2022).
[60] W. E. East and J. L. Ripley, Phys. Rev. D **103**, 044040 (2021).
[61] J. L. Ripley, J. Mod. Phys. D **31**, 2230017 (2022).
[62] M. Corman, J. L. Ripley, and W. E. East, Phys. Rev. D **107**, 024014 (2023).
[63] L. Aresté Saló, K. Clough, and P. Figueras, Phys. Rev. Lett. **129**, 261104 (2022).
[64] L. Aresté Saló, K. Clough, and P. Figueras, Phys. Rev. D **108**, 084018 (2023).
[65] H. Witek, L. Gualtieri, P. Pani, and T. P. Sotiriou, Phys. Rev. D **99**, 064035 (2019).
[66] H. O. Silva, H. Witek, M. Elley, and N. Yunes, Phys. Rev. Lett. **127**, 031101 (2021).
[67] M. Okounkova, Phys. Rev. D **102**, 084046 (2020).
[68] H.-J. Kuan, A. T.-L. Lam, D. D. Doneva, S. S. Yazadjiev, M. Shibata, and K. Kiuchi, Phys. Rev. D **108**, 063033 (2023).
[69] M. Corman, L. Lehner, W. E. East, and G. Dideron, arXiv:2405.15581.
[70] A. D. Kovacs and H. S. Reall, Phys. Rev. Lett. **124**, 221101 (2020).
[71] A. D. Kovacs and H. S. Reall, Phys. Rev. D **101**, 124003 (2020).
[72] J. L. Ripley and F. Pretorius, Phys. Rev. D **101**, 044015 (2020).
[73] P. Pani, E. Berti, V. Cardoso, and J. Read, Phys. Rev. D **84**, 104035 (2011).
[74] J. L. Ripley and F. Pretorius, Classical Quantum Gravity **36**, 134001 (2019).
[75] J. L. Ripley and F. Pretorius, Phys. Rev. D **99**, 084014 (2019).
[76] J. L. Ripley and F. Pretorius, Classical Quantum Gravity **37**, 155003 (2020).
[77] W. E. East and J. L. Ripley, Phys. Rev. Lett. **127**, 101102 (2021).
[78] W. E. East, F. Pretorius, and B. C. Stephens, Phys. Rev. D **85**, 124010 (2012).
[79] W. E. East, F. Pretorius, and B. C. Stephens, Phys. Rev. D **85**, 124009 (2012).
[80] F. Pretorius, B. Stephens, and M. W. Choptuik, PAMR, http://laplace.physics.ubc.ca/Group/Software.html.
[81] L. J. Papenfort, S. D. Tootle, P. Grandclément, E. R. Most, and L. Rezzolla, Phys. Rev. D **104**, 024057 (2021).
[82] P. Grandclement, J. Comput. Phys. **229**, 3334 (2010).
[83] M. Okounkova, L. C. Stein, J. Moxon, M. A. Scheel, and S. A. Teukolsky, Phys. Rev. D **101**, 104016 (2020).
[84] J. S. Read, B. D. Lackey, B. J. Owen, and J. L. Friedman, Phys. Rev. D **79**, 124032 (2009).
[85] M. Alford, M. Braby, M. W. Paris, and S. Reddy, Astrophys. J. **629**, 969 (2005).
[86] A. Gonzalez *et al.*, Classical Quantum Gravity **40**, 085011 (2023).
[87] H. T. Cromartie *et al.* (NANOGrav Collaboration), Nat. Astron. **4**, 72 (2019).
[88] T. E. Riley *et al.*, Astrophys. J. Lett. **918**, L27 (2021).
[89] M. H. van Kerkwijk, R. P. Breton, and S. R. Kulkarni, Astrophys. J. **728**, 95 (2011).
[90] E. Fonseca *et al.*, Astrophys. J. **832**, 167 (2016).
[91] J. Antoniadis *et al.*, Science **340**, 6131 (2013).
[92] B. Margalit and B. D. Metzger, Astrophys. J. Lett. **850**, L19 (2017).
[93] D. Radice, A. Perego, F. Zappa, and S. Bernuzzi, Astrophys. J. Lett. **852**, L29 (2018).
[94] B. P. Abbott *et al.* (LIGO Scientific and Virgo Collaborations), Phys. Rev. X **9**, 011001 (2019).
[95] P. T. H. Pang, I. Tews, M. W. Coughlin, M. Bulla, C. Van Den Broeck, and T. Dietrich, Astrophys. J. **922**, 14 (2021).
[96] M. W. Coughlin, T. Dietrich, B. Margalit, and B. D. Metzger, Mon. Not. R. Astron. Soc. **489**, L91 (2019).
[97] D. Radice and L. Dai, Eur. Phys. J. A **55**, 50 (2019).
[98] B. P. Abbott *et al.* (LIGO Scientific and Virgo Collaborations), Phys. Rev. Lett. **119**, 161101 (2017).
[99] H. Tan, J. Noronha-Hostler, and N. Yunes, Phys. Rev. Lett. **125**, 261104 (2020).
[100] M. Fasano, K. W. K. Wong, A. Maselli, E. Berti, V. Ferrari, and B. S. Sathyaprakash, Phys. Rev. D **102**, 023025 (2020).
[101] H. Yasin, S. Schäfer, A. Arcones, and A. Schwenk, Phys. Rev. Lett. **124**, 092701 (2020).
[102] A. Bauswein, H. T. Janka, and R. Oechslin, Phys. Rev. D **82**, 084043 (2010).
[103] S. E. Perkins, R. Nair, H. O. Silva, and N. Yunes, Phys. Rev. D **104**, 024060 (2021).
[104] J. L. Blázquez-Salcedo, C. F. B. Macedo, V. Cardoso, V. Ferrari, L. Gualtieri, F. S. Khoo, J. Kunz, and P. Pani, Phys. Rev. D **94**, 104024 (2016).
[105] L. Pierini and L. Gualtieri, Phys. Rev. D **103**, 124017 (2021).
[106] L. Pierini and L. Gualtieri, Phys. Rev. D **106**, 104009 (2022).

[107] C. Reisswig and D. Pollney, Classical Quantum Gravity **28**, 195015 (2011).
[108] D. Christodoulou, Phys. Rev. Lett. **25**, 1596 (1970).
[109] F.-L. Julié, V. Baibhav, E. Berti, and A. Buonanno, Phys. Rev. D **107**, 104044 (2023).
[110] P. C. Peters and J. Mathews, Phys. Rev. **131**, 435 (1963).
[111] E. Berti, V. Cardoso, J. A. Gonzalez, U. Sperhake, M. Hannam, S. Husa, and B. Bruegmann, Phys. Rev. D **76**, 064034 (2007).
[112] M. Maggiore, *Gravitational Waves. Vol. 1: Theory and Experiments*, Oxford Master Series in Physics (Oxford University Press, New York, 2007).
[113] L. Bernard, L. Blanchet, and D. Trestini, J. Cosmol. Astropart. Phys. 08 (2022) 008.
[114] F.-L. Julié, L. Pompili, and A. Buonanno, arXiv:2406.13654.
[115] E. E. Flanagan and T. Hinderer, Phys. Rev. D **77**, 021502 (2008).
[116] I. van Gemeren, B. Shiralilou, and T. Hinderer, Phys. Rev. D **108**, 024026 (2023).
[117] L. Bernard, E. Dones, and S. Mougiakakos, Phys. Rev. D **109**, 044006 (2024).
[118] N. Yunes and F. Pretorius, Phys. Rev. D **80**, 122003 (2009).
[119] S. Perkins and N. Yunes, Phys. Rev. D **105**, 124047 (2022).
[120] A. K.-W. Chung and N. Yunes, arXiv:2405.12280.
[121] F. Foucart, T. Hinderer, and S. Nissanke, Phys. Rev. D **98**, 081501 (2018).
[122] S. Biscoveanu, P. Landry, and S. Vitale, Mon. Not. R. Astron. Soc. **518**, 5298 (2022).
[123] T. Evstafyeva, M. Agathos, and J. L. Ripley, Phys. Rev. D **107**, 124010 (2023).
[124] E. Maggio, H. O. Silva, A. Buonanno, and A. Ghosh, Phys. Rev. D **108**, 024043 (2023).
[125] V. Gennari, G. Carullo, and W. Del Pozzo, Eur. Phys. J. C **84**, 233 (2024).
[126] A. Maselli, P. Pani, L. Gualtieri, and E. Berti, Phys. Rev. D **101**, 024043 (2020).
[127] A. Ghosh, R. Brito, and A. Buonanno, Phys. Rev. D **103**, 124041 (2021).
[128] H. O. Silva, A. Ghosh, and A. Buonanno, Phys. Rev. D **107**, 044030 (2023).
[129] G. Carullo, Phys. Rev. D **103**, 124043 (2021).
[130] S. Chen, L. Wang, K. Hayashi, K. Kawaguchi, K. Kiuchi, and M. Shibata, Phys. Rev. D **110**, 063016 (2024).
[131] T. Martineau, F. Foucart, M. Scheel, M. Duez, L. Kidder, and H. Pfeiffer, arXiv:2405.06819.
[132] https://www.scinethpc.ca/.
[133] https://alliancecan.ca/en.